POLITECNICO
MILANO 1863

SCUOLA DI INGEGNERIA INDUSTRIALE
E DELL'INFORMAZIONE

Executive Summary of the Thesis

Loudspeaker Motor: Design and Non-Ideality Analysis

Laurea Magistrale in Music and Acoustic Engineering - Ingegneria Acustica e Musicale

Author: Marco Cafaro

Advisor: Prof. Giuseppe Bertuccio

Co-advisor: Grazia Spatafora, PhD.

Academic year: 2021-2022

---

1. Introduction

Loudspeakers have been used for many years to convert electrical audio signals into sound waves. The basis of the loudspeaker is the electromotive force, also known as *Lorentz force*, which an electrical conductor in a perpendicular magnetic field experiences when an electrical current is passed through it. In most electrodynamic transducers, the conductor consists in a *moving coil* placed inside a magnetic field generated by the *magnetic circuit*. The latter is composed by the permanent *magnet* and the *soft iron parts* that guide the magnetic flux generated by the magnet to the *air gap*.
The *cone*, attached to the moving coil, transforms this movement into air pressure waves, while the *suspensions* provide the recall forces that keep the moving parts in the rest position. In this thesis we will focus only on the transducer motor, composed by the magnetic circuit and the moving coil. The studied motor configuration is the magnet ring type. For detailed descriptions of each motor component i refer to [2].
The Thiele-Small (T-S) lumped-element model is commonly used by driver manufacturers to describe quite well the loudspeaker behaviour. It can be shown that the electrical impedance of the model can be divided into *mechanical impedance* and *blocked impedance*. The blocked impedance is defined as the electrical impedance when the voice coil is blocked in the air gap, and is related to the motor electromagnetic features. Many other blocked impedance models have been added in the literature, expanding the simple resistor-inductor introduced by Small, which does not fit the measurements. The most important are the ones introduced by Wright, Leach [4] and Klippel [3]. Klippel's LR-2 model is commonly used in commercial measurement setups and R&D departments.
Besides these models, it can be difficult to predict the effect of the motor non-idealities on the blocked impedance during the loudspeaker initial design phases. Thus, many engineers started to find other solutions by means of much more powerful and complex tools such as Finite Element Method (FEM) software. In the loudspeaker industry, FEM software are used to study separately and jointly the acoustical, mechanical and electromagnetic features of the transducer.
An important and current research topic, with significant implication in the design of loudspeakers for high-quality audio system, is related to the audio signal distortion due to non linearities in the electro-mechano-acoustic

transduction: the main distortion source is related to the suspensions for most of the audio frequency spectrum. However, motor non-linearities should not be overlooked and will be the focal point of this work. Baratelli and Munroe's work [1] is reported as an example, in which they simulated the harmonic distortion in the electrical current flowing through a loudspeaker's blocked coil, comparing different hysteresis models for the iron plates to solve the problem.
The three main distortion causes in the loudspeaker motor are:

- the force factor $Bl(x)$ depends on the voice coil position, introducing distortion at major displacements;
- the voice coil inductance $L_E(x)$ depends also on the coil position;
- flux modulation generated by AC currents inside the iron changes the coil inductance $L_E(i)$ depending on the current amplitude, and introducing distortion in the coil current;

Changes in loudspeaker motor performance are also due to components mechanical tolerances, their influence is important to check to guarantee repeatability during production and high product performances.

2. Aim

The thesis target is to develop robust FEM models capable to predict efficiently and accurately the electromagnetic loudspeakers motor parameters and variables needed for loudspeaker design. The main motor non-idealities are analysed and discussed, such as causes of non-linear distortion and performance deviations derived by geometric tolerances. In particular, the displacement dependent force factor $Bl(x)$, blocked impedance $Z_E(x, f)$ and the total harmonic distortion (THD) in the blocked coil are evaluated. The geometric dimensions influence of the magnetic circuit is assessed through the use of quick numerical models. Finally, we will discuss the effect of the mechanical tolerances on the output force factor and impedance performances.
Ad hoc measurement setups have been developed to validate FEM models. Three different loudspeakers of different sizes in blocked coil condition are measured and simulated. The blocked coil condition allow us to neglect the motional part of the electro-mechanical transduction, focusing only on the motor. All simulation models are settled up with the COMSOL®Multiphysics software and processed with MATLAB®.

3. Materials and Methods

Three different loudspeaker prototypes, chosen accordingly to their motor size and demodulation characteristics[1] are simulated and measured:

- *Motor #1* is a 3-inch full range[2] woofer motor. Ferrite magnet and copper cap.
- *Motor #2* is a 6-inch mid range[2] woofer motor. Neodymium magnet and aluminium ring under the upper plate.
- *Motor #3* is a 15-inch bass[2] woofer motor. Neodymium magnet and aluminium ring.

3.1. FEM Analyses

3.1.1 Magneto-static analysis

The magneto-static (MS) analysis focus on the static magnetic flux generated by the magnet. The solved equations are derived directly by Maxwell's equations in a static regime. The MS analysis is used to evaluate the main performances of the magnetic circuit such as the magnetic flux and permeability in the steel and the magnet working point. The latter corresponds to the intersection between the magnet BH demagnetization curve and its load state, defined as the magnetic flux generated by the magnet. This information tells how well the magnet is exploited and if it is in risk to be demagnetized by external agents. The $Bl(x)$ curve is also evaluated. It is useful to define the symmetry index $S.I.$ as eq.1:

$$S.I.= \left(1- \sqrt{\frac{1}{N} \cdot \sum_{j=1}^{N} \left(2 \cdot \frac{Bl(x_j)-Bl(-x_j)}{Bl(x_j)+Bl(-x_j)} \right)^2} \right) \cdot 100\% \quad (1)$$

where N is the number of displacement points evaluated. The $S.I.$ tells how much symmetric a curve is (in percentage), being $S.I. = 100\%$ for a perfect symmetry $Bl(x) = Bl(-x)$.

[1] Each prototype features a demodulation component, such a metallic ring or cap that help reduce the magnetic flux modulation and more.

[2] These terms refer to the audio frequency range of the woofer output sound.

3.1.2 Small signal analysis

The small signal (SS) analysis is a frequency domain perturbation analysis used for studying small oscillations around a biased solution. It is used to evaluate the effects of a small time harmonic signal without considering any sort of non-linearity. The blocked impedance $Z_E(x, f)$ is retrieved. For graphical purposes, it is useful to represent the impedance through the Leach's model [4]. The effective resistance and inductance are related to the blocked impedance $Z_E(x, f)$ as follows in eq.2 and eq.3:

$$R_{eff}(x, f) = \Re\big(Z_E(x, f)\big) \tag{2}$$

$$L_{eff}(x, f) = \frac{\Im\big(Z_E(x, f)\big)}{2\pi f} \tag{3}$$

L_{eff} is always positive by model definition.

3.1.3 Large signal analysis

To consider the non-linear distortion sources, a time domain analysis is required. With the large signal (LS) analysis, the THD in the blocked voice coil is evaluated for many driving voltages. The first three harmonics of the current spectrum are extracted by performing a modified periodogram using a Kaiser window with large sidelobe attenuation ($\beta = 38$).

3.1.4 MS Local sensitivity analysis

Sensitivity analysis (SA) is a method that measures how the impact of tolerances of one or more input parameters can lead to variation on the output variables. In this work i propose a local SA method applied to the magnetic circuit geometry parameters in relation to the force factor, and study their effects on the force factor $Bl(x = 0)$. The definition of local sensitivity of a scalar objective function $Q(\xi)$ with respect to the control variables ξ at a specific point ξ_0 is given in eq.4:

$$S_{Q(\xi)} = \left.\frac{\partial Q}{\partial \xi}\right|_{\xi_0} \tag{4}$$

This analysis is an expansion of the MS analysis.

3.1.5 Parametric MS/SS analysis

The parametric analysis is used to investigate the relation of the parameters that affect most the Bl and Z_E output variables. The local sensitivity analysis is used as a *screening* stage. Once individuated the most significant parameters, multiple magneto-static and small signal analyses are executed considering every possible combination of the selected parameters. Then, the output variables of interest are evaluated in terms of deviation from the nominal configuration, as described by eq.5:

$$\mathrm{dev}_Q(\vec{\xi_k}) = \frac{Q(\vec{\xi_k}) - Q(\vec{\xi}_{nm})}{Q(\vec{\xi}_{nm})} \cdot 100\% \tag{5}$$

where $Q(\vec{\xi_k})$ is the output variable related to the input parameters combination $\vec{\xi_k}$; vector $\vec{\xi}_{nm}$ contains the nominal configuration parameters.

3.2. FEM models description

Models are settled up in 2D-axisymmetric models. Metal basket is included for a more accurate prediction of the real environment. An outer semicircular layer is designed to represent the *infinite domains*.
Copper and aluminium components are treated as linear conductive medium without magnetic properties. Air electric conductivity is set to be negligible.
Magnets are modelled by the constitutive relation described in eq.6:

$$\vec{B} = \mu_0 \mu_{rec} \vec{H} + \vec{B}_r \tag{6}$$

where μ_0 is the vacuum permeability, μ_{rec} the recoil permeability of the magnet and $\vec{B}_r$ its remanent flux density. These values are retrieved from the hysteresis graph measurement.
The polar plates are all made of steel, modelled by relating directly the magnetic flux density $\vec{B}$ and the magnetic field $\vec{H}$ as $|\vec{H}| = f(|\vec{B}|)$, using the steel magnetization curves. Such curves have been measured by an external laboratory, and fitted to further extend their utility in the saturation region.
Plates are zinc-plated to prevent corrosion. This zinc layer could interfere with eddy currents at high frequencies when the skin depth is comparable to the layer thickness. For such reason, zinc layers are modelled through the use of transition boundary conditions, without creating such small domains that could increase the number of mesh elements.
An appropriate mesh is applied to each motor geometry, with particular attention to the

eddy currents: a layer of three elements is distributed on the steel components boundaries, which varies with frequency according to the skin depth.
The magneto-static analysis is carried out multiple times by changing the voice coil position each time, for the $Bl(x)$ curve evaluation.
The same thing is applied to the small signal analysis, which evaluates the position dependent $Z_E(x, f)$. Additionally, each study step is swept on the frequency axis in the audio spectrum $20-20000$Hz.
The large signal analysis model is the direct mirror of the related measurement setup: to best fit the measurements, an external circuit representing the setup is implemented in the numerical model. The time domain simulation is carried out over a single sinusoidal stimulus multiple times in the frequency range of interest. This procedure is repeated for many driving voltages at the coil terminals.
The local sensitivity analysis is implemented by deforming the mesh elements on the boundaries related to the geometry parameters. Sensitivity values are computed by performing small oscillations around the nominal dimensions.
Finally, the parametric analysis is performed on the selected most significant parameters from the local SA, by repeating magneto-static and small signal analyses for each parameter combination for a total of 1944 study steps per prototype.

3.3. Measurements

In this summary, measurement setups will not be described. Anyway, the most useful results from each measurement are:

- *Hall sensor scanning*: the average magnetic flux in the air gap,
- *Magnet hysteresis graph*: Magnet demagnetizing curve, energy product curve and remanence B_r,
- *Klippel LSI (large signal identification)*: force factor curve $Bl(x)$,
- *Klippel TRF (transfer function measurement)*: THD plots of the complete woofer (with mechanical components), shown in Figure 1,
- *Blocked impedance measurements*: Blocked impedance $Z_E(x, f)$ on five different voice coil positions,

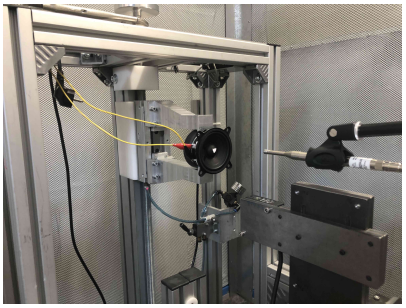

Figure 1: Kippel TRF measurement.

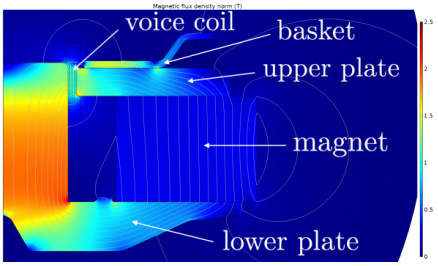

Figure 2: 2D view of the magnetic flux density distribution of *motor #1*.

- *Current distortion measurements*: current distortion harmonics in the blocked voice coil (at rest position).

4. Results and Discussion

Only partial results are presented. More details and results are reported in the Thesis.

4.1. Magneto-static analysis

In this section, the magnetic circuit performances and the force factor curve are reported and discussed. Figure 2 shows the magnetic flux density distribution of *motor #1*. We can see that the pole piece steel is saturated, meaning that will be less affected by flux modulation. The working point of the magnet is above the maximum of the energy product function (Figure 3): this strengthen the working point versus low temperature demagnetization and flux modulation. The measured and simulated $Bl(x)$ curves are compared in Figure 4, showing excellent agreement.

4.2. Small signal analysis

The simulated blocked impedance at rest position of *motor #2* is validated by measurements in Figure 5. Figure 6 compares the simulated and measured apparent resistance and inductance of the voice coil positioned in five different

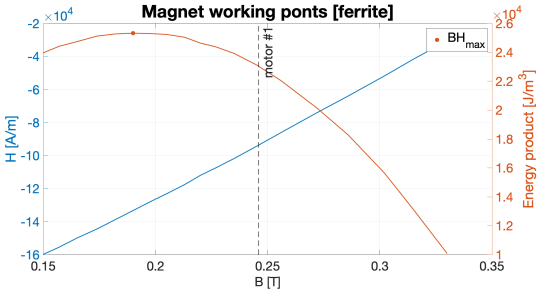

Figure 3: Measured characteristic demagnetization curves and energy product of the ferrite magnet. The simulated working point of *motor #1* is reported.

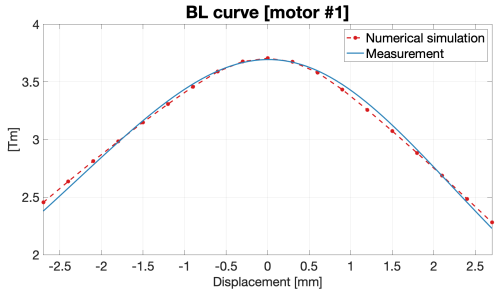

Figure 4: $Bl(x)$ curves comparison between simulations and measurements (*motor #1*).

positions. It is shown how the impedance varies with coil displacement. The inductive part is reasonably lower when the coil is almost out of the air gap.

4.3. Large signal analysis

Figure 7 compares the measured and simulated fundamental (H1), 2^{nd} (H2) and 3^{rd} (H3) harmonics of the current spectrum. Results show an acceptable prediction of H1 and H2, but almost all simulations show a different behaviour of H3. The measured current THD levels are then compared with the THD values of the whole trans-

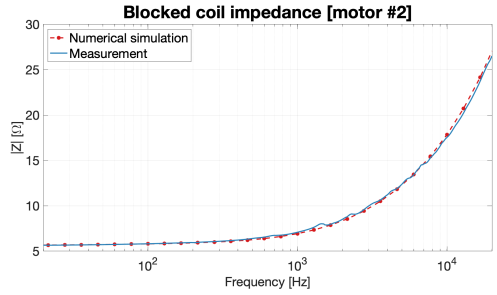

Figure 5: Measured and simulated blocked impedance of *motor #2* (in rest position).

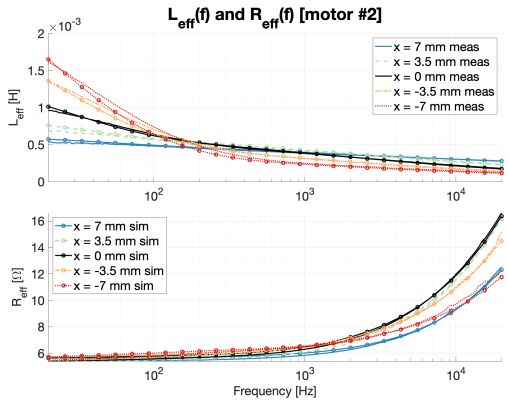

Figure 6: Measured (lines) and simulated (points) effective inductance $L_{eff}(x,)$ and resistance $R_{eff}(x,f)$ at different voice coil displacements (*motor #2*).

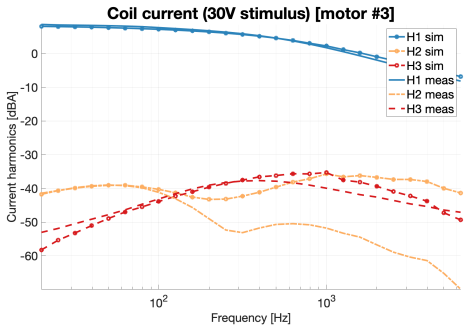

Figure 7: Simulated and measured current harmonics with 30V peak voltage at coil terminals (*motor #3*).

ducer, confirming its relevance in the mid-audio range. For example, at 30 V the THD of the current in *motor #3* is $\sim 0.75\%$, which is half the overall THD of the transducer ($\sim 1.47\%$).

4.4. MS Local sensitivity analysis

Magneto-static local sensitivity analysis is performed using $Bl(0)$ as objective function. Figure 8 reports geometrical parameters of *motor #1*. As expected, geometrical parameters related to air gap dimensions have the highest influence, where $BL(0)$ sensitivity values are 1.8 and -1.5 T m mm^{-1} respectively for r_1 and r_5. The magnet dimensions are less relevant when compared to the other motor geometries due to the high energy product of neodymium. For example, *motor #1* inner magnet radius r_3 and magnet height z_3 have a $BL(0)$ sensitivity equal to -5.7×10^{-2} and 6.7×10^{-2} T m mm^{-1}, while *motor #2* counterparts are one order of magni-

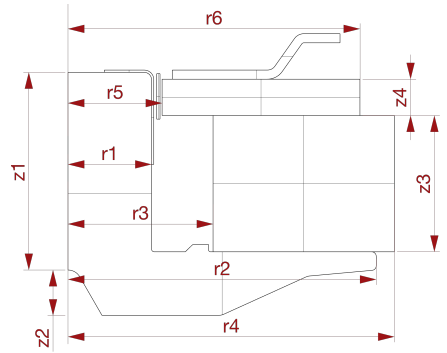

Figure 8: 2D representation of *motor #1*, which shows the geometric parameters involved in the local sensitivity analysis.

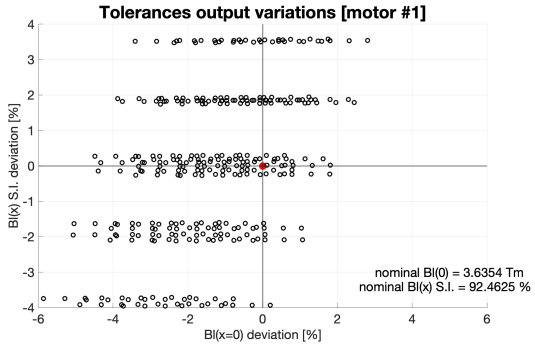

Figure 9: Tolerances force factor variations (*motor #1*). Each point references to a different parameters combination.

tude higher (i.e. -2.7×10^{-1} and 5.8×10^{-1} $\mathrm{T\,m\,mm^{-1}}$). These results are also confirmed by the mechanical tolerances chosen for these geometrical parameters: r_1 e r_3 have restricted tolerances (i.e. $[-0.025, 0]$ and $[0, +0.025]$ mm) while r_3 and z_3 uncertainties lay in a wider range (i.e. $[-0.35, +0.35]$ and $[-0.1, +0.1]$ mm).

4.5. Parametric MS analysis

The result is shown through the use of a scatter plot, where two main quality factors ($Bl(0)$ and $S.I.$) determine the location of each parameters combination (point) as shown in Figure 9. In this way we can locate the region with best and worst combinations as respectively the first and third quadrant. We can see that most of the combinations have worse performances in respect to the nominal configuration. It is estimated that this variance of force factor produces an output SPL 1W/1m deviation between $-0.54\,\mathrm{dB}$ and $0.26\,\mathrm{dB}$, considered acceptable.

5. Conclusion and Future Works

The essential design parameters of the transducer motor have been accurately predicted through quick and efficient numerical magnetostatic/small signal analyses on three different prototype geometries. The main distortion causes in the motor are assessed, such as the displacement dependent force factor and blocked impedance, validating the simulations with measurements. The current THD is evaluated and discussed along with measurements: a better hysteresis model or a 3D approach is needed to correctly predict the third harmonic, but would further increase its high computational times and complexity. The local sensitivity analysis evaluated quickly the most significant geometry parameters, remarking its usefulness in the tolerancing stage. Parametric solutions showed how the mechanical tolerances affect the force factor and blocked impedance. However, assembling tolerances remain to be explored.
Further developments have been started but are not covered in this thesis, regarding optimization algorithms of the polar plates shapes which are useful to reduce cost and save up material.

6. Acknowledgements

The author would like to thank Romolo Toppi and Grazia Spatafora from Faital S.p.A., and prof. Giuseppe Bertuccio for their help and support in completing this thesis.

References

[1] M. Baratelli and O. Munroe. Predicting loudspeaker current distortion with fea. *Journal of the Audio Engineering Society*, may 2020.

[2] J. Eargle. *Loudspeaker Handbook*. Springer US, 2003.

[3] W. Klippel. Tutorial: Loudspeaker nonlinearities—causes, parameters, symptoms. *J. Audio Eng. Soc*, 54(10):907–939, 2006.

[4] W. M. Leach, jr. Loudspeaker voice-coil inductance losses: Circuit models, parameter estimation, and effect on frequency response. *Journal of the Audio Engineering Society*, 50(6):442–450, June 2002.